

Chaotic motion of scalar particle coupling to Chern-Simons invariant in the stationary axisymmetric Einstein-Maxwell dilaton black hole spacetime

Lina Zhang^{1,2}, Songbai Chen^{1,2,3*}, Qiyuan Pan^{1,2,3†}, and Jiliang Jing^{1,2,3 ‡}

¹*Key Laboratory of Low Dimensional Quantum Structures and Quantum Control of Ministry of Education, Synergetic Innovation Center for Quantum Effects and Applications,*

and Department of Physics, Hunan Normal University, Changsha, Hunan 410081, China

²*Institute of Interdisciplinary Studies, Hunan Normal University, Changsha, Hunan 410081, China and*

³*Center for Gravitation and Cosmology, College of Physical Science and Technology, Yangzhou University, Yangzhou 225009, China*

Abstract

We investigate the motion of a test scalar particle coupling to the Chern-Simons (CS) invariant in the background of a stationary axisymmetric black hole in the Einstein-Maxwell-Dilaton-Axion (EMDA) gravity. Comparing with the case of a Kerr black hole, we observe that the presence of the dilation parameter makes the CS invariant more complex, and changes the range of the coupling parameter and the spin parameter where the chaotic motion appears for the scalar particle. Moreover, we find that the coupling parameter together with the spin parameter also affects the range of the dilation parameter where the chaos occurs. We also probe the effects of the dilation parameter on the chaotic strength of the chaotic orbits for the coupled particle. Our results indicate that the coupling between the CS invariant and the scalar particle yields the richer dynamical behavior of the particle in the rotating EMDA black hole spacetime.

PACS numbers: 04.70.-s, 04.70.Bw, 97.60.Lf

* csb3752@hunnu.edu.cn

† panqiyuan@hunnu.edu.cn

‡ jljing@hunnu.edu.cn

I. INTRODUCTION

Chaos is a kind of very interesting motions occurred in nonlinear dynamical systems. The main feature of chaos is its high sensitivity to initial conditions, so tiny differences in initial conditions grow at exponential rates and lead to totally different states of motion [1–3]. This means that a long-term prediction to the motion is very difficult for a chaotic dynamical system. Therefore, the effects from nonlinear interactions yield that chaotic systems have a lot of novel properties, which are not shared by the linear dynamical systems. This also triggers much efforts being devoted to studies of chaos in various physical fields.

In general relativity, to probe the chaotic motions of particles, one must resort to some spacetimes with complex geometrical structures or introduce some extra interactions to ensure that the dynamical system of particles is non-integrable. In this way, the chaotic orbits of particles have been investigated in the multi-black hole spacetime [4], or in a black hole spacetime immersed in a magnetic field [5], or in an accelerating and rotating black hole spacetime [6]. Recently, by introducing an extra interaction with the Einstein tensor, the chaotic dynamics of a scalar test particle in the Schwarzschild-Melvin black hole spacetime has been studied [7]. Additionally, the thermal chaos in the extended phase space has been studied in the spacetimes of a charged AdS black hole in various theories of gravity [8–11].

Although Einstein’s general theory of relativity has passed all current observational and experimental tests [12], it is widely recognized that it may not be the ultimate theory describing gravitational fields. Instead, it could be a valid description of an unknown fundamental theory of gravity [13]. Therefore, there is great interest in studying potential extensions to Einstein’s general relativity. One of the most promising alternative gravity theories is the dynamical CS modified gravity [14], where the Einstein-Hilbert action is modified by adding an extra interaction between the scalar field and the CS invariant. This interaction captures the leading-order gravitational parity violation. Generally, it is not easy to get an analytical black hole solution in the dynamical CS gravity because both motion equations of gravitational and scalar fields must be satisfied simultaneously. Thus, the analytical solution of a rotating black hole in this modified gravity has been obtained only in the small-coupling and/or slow-rotation limit [15–20]. Recently, a CS scalar field induced by a rapidly rotating black hole in the dynamical CS modified gravity has been also investigated in [21], and it is shown that the scalar field diverges on the inner horizon although it is regular on the outer horizon and vanishes at infinity, which means that the CS scalar field becomes problematic on the inner horizon.

Only the linear coupling is discussed in above literatures on the dynamical CS gravity, where the coupling

term with the CS invariant is proportional to the scalar field. Inspired by the theoretical model in the quadratic scalar-Gauss-Bonnet gravity [22–24], the model where the CS invariant is coupled to the quadratic function of the dynamical scalar field has been investigated in [25], and it is found that the scalar perturbation around a Kerr black hole grows at exponential rate in a certain regions of the parameter space, which means that the black hole could be unstable under such CS scalar perturbation. With the short wave approximation study, Zhou et al. [26] studied the effects of such quadratic coupling on the motion of a test scalar particle in a Kerr black hole background, and found that there exists the chaotic phenomenon in the motion of the scalar particle coupling to the CS invariant. It is natural to ask whether there exists the chaos in the motion of the scalar particle in other rotating black hole spacetimes under such kind of couplings. The EMDA black hole is an important black hole in the EMDA gravity, which is regraded as the low energy limit of the heterotic string theory [27]. This black hole is characterized by its mass, spin and dilation parameters. Since the string theory is the present strongest candidate for the quantum description of gravity, the EMDA black hole has been widely studied in various aspects. In this paper, we want to study the effects of such quadratic coupling on the motion of a test scalar particle in a EMDA black hole background [27] and probe effects of the coupling parameter together dilation parameter on the motion of the scalar particle coupling to the CS invariant.

The paper is organized as follows. In Sec. 2, we adopt the short-wave approximation as in [26] and present the geodesic equation of a test scalar particle coupling to the CS invariant in the EMDA black hole spacetime. In Sec. 3, we investigate the chaotic motion of the coupled scalar particle with the Poincaré section, the fast Lyapunov indicator (FLI), the bifurcation diagram and the basins of attraction. We probe the effects of this coupling together with the black hole dilation and spin parameters on the chaotic behavior of the coupled scalar particle. Finally, we end the paper with a summary.

II. GEODESICS OF SCALAR PARTICLE COUPLING TO CHERN-SIMONS INVARIANT IN THE STATIONARY AXISYMMETRIC EMDA BLACK HOLE

In the theory of Einstein-Maxwell dilation gravity, the action containing the coupling between the CS invariant and the quadratic function of a scalar perturbational field can be expressed as [25]

$$S = \int d^4x \sqrt{-g} \left(\frac{R}{16\pi G} - \frac{1}{2} g^{\mu\nu} \partial_\mu \phi \partial^\mu \phi - \frac{1}{4} e^{-2\phi} F^{\mu\nu} F_{\mu\nu} - \frac{1}{2} g^{\mu\nu} \partial_\mu \Phi \partial^\mu \Phi - \mu^2 \Phi^2 + \alpha {}^*RR\Phi^2 \right), \quad (1)$$

where R is the Ricci scalar and G is the usual Newton's constant. ϕ is a massless dilaton field and Φ is a massive scalar perturbational field with the mass μ . The CS invariant *RR is defined by

$${}^*RR = \frac{1}{2} \epsilon^{\alpha\beta\gamma\delta} R^\mu_{\nu\gamma\delta} R^\nu_{\mu\alpha\beta}, \quad (2)$$

which is a topological invariant. $\epsilon^{\alpha\beta\gamma\delta}$ is the four-dimensional Levi-Civita tensor and $R^\mu_{\nu\gamma\delta}$ is the Riemann curvature tensor. The coupling parameter α has a dimension of length squared and describes the strength of the coupling between the scalar perturbational field and the CS invariant. Varying the action (1) with respect to the field Φ , one can obtain the modified Klein-Gordon equation for the scalar perturbation

$$\frac{1}{\sqrt{-g}} \frac{\partial}{\partial x^\mu} \left(\sqrt{-g} g^{\mu\nu} \frac{\partial \Phi}{\partial x^\nu} \right) + (2\alpha^* RR - \mu^2) \Phi = 0. \quad (3)$$

As discussed in [26], we here adopt the short wave approximation for the scalar perturbational field Φ and derive the equation of motion for scalar particle in a background spacetime. In the short wave approximation, the wavelength of the scalar perturbational field is assumed to be much smaller than the typical curvature of the spacetime, so the particle aspect of the scalar field is dominated and its wave aspect can be neglected. With this approximation, the scalar perturbational field Φ can be further reduced to

$$\Phi = f e^{iS}, \quad (4)$$

where the amplitude f is a small slowly-varying real and the phase S is rapidly changing. Therefore, the derivative term $f_{;\mu}$ can be ignored because it is not dominated in this case. The wave vector $\partial_\mu S$ can be regarded as the momentum p_μ of the corresponding scalar particle. And then the modified Klein-Gordon equation (3) can be rewritten as

$$g^{\mu\nu} p_\mu p_\nu - 2\alpha^* RR = -1. \quad (5)$$

Setting the mass of the scalar particle be $\mu = 1$, the equation (5) can be rewritten as a form of Hamilton-Jacobi equation

$$\frac{\partial S}{\partial \tau} + \mathcal{H} \left(x^\mu, \frac{\partial S}{\partial x^\mu} \right) = 0, \quad (6)$$

where $S = \frac{1}{2}\tau + x^\mu p_\mu$ and the corresponding Hamiltonian is

$$\mathcal{H} \left(x^\mu, \frac{\partial S}{\partial x^\mu} \right) = \frac{1}{2} g^{\mu\nu} p_\mu p_\nu - \alpha^* RR. \quad (7)$$

Here x^μ and p_μ , respectively represent the spacetime coordinates and the canonical momentum of the scalar field. τ is an affine parameter along a curve. The term $-\alpha^* RR$ can be treated as an extra potential from the interaction between the scalar particle and the CS invariant.

In the Boyer-Lindquist coordinates (t, r, θ, φ) , the solution of the stationary axisymmetric EMDA black hole

has a form [27–30]

$$ds^2 = -\frac{\Sigma - a^2 \sin^2 \theta}{\Delta} dt^2 - \frac{2a \sin^2 \theta}{\Delta} [(r^2 - 2Dr + a^2) - \Sigma] dt d\varphi + \frac{\Delta}{\Sigma} dr^2 + \Delta d\theta^2 + \frac{\sin^2 \theta}{\Delta} [(r^2 - 2Dr + a^2)^2 - \Sigma a^2 \sin^2 \theta] d\varphi^2, \quad (8)$$

with

$$\Sigma = r^2 - 2Mr + a^2, \quad \Delta = r^2 - 2Dr + a^2 \cos^2 \theta, \quad (9)$$

where M , D and a represent the mass, dilaton and angular momentum per unit mass of the black hole, respectively. The Arnowitt-Deser-Misner (ADM) mass of the black hole (8) is $M_{ADM} = M - D$. The outer and inner horizons are located at $r_{\pm} = M_{ADM} + D \pm \sqrt{(M_{ADM} + D)^2 - a^2}$. The CS invariant for the black hole (8) is

$${}^*RR = \frac{32a(M - D) \cos \theta (a^2 \cos^2 \theta + 2Dr - 3r^2)}{(a^2 \cos^2 \theta - 2Dr + r^2)^6} \{a^2 \cos^2 \theta [2D^2 - 3D(M + 3r) + 9Mr] - 2D^2(Mr + r^2 - a^2) + 3r^2(DM + Dr - Mr)\}. \quad (10)$$

When $D = 0$, the invariant reduces to that in the Kerr black hole. As in the Kerr case, the CS invariant *RR (10) also contains the linear term of $\cos \theta$, and it's asymmetrical to the equatorial plane. The chaotic motion of the scalar particle coupling to the CS invariants in the Kerr spacetime has been investigated in [26]. Here, we will study the effects of the dilaton parameter D on the motion of the coupled scalar particles.

From the Hamiltonian (7), one can get the geodesic equation for the coupled scalar particle

$$\dot{t} = \frac{g_{\varphi\varphi} E + g_{t\varphi} L_z}{g_{t\varphi}^2 - g_{tt} g_{\varphi\varphi}}, \quad \dot{\varphi} = -\frac{g_{t\varphi} E + g_{tt} L_z}{g_{t\varphi}^2 - g_{tt} g_{\varphi\varphi}}, \quad (11)$$

and

$$\ddot{r} = \frac{1}{2} g^{rr} \left(g_{tt,r} \dot{t}^2 - g_{rr,r} \dot{r}^2 + g_{\theta\theta,r} \dot{\theta}^2 + g_{\varphi\varphi,r} \dot{\varphi}^2 + 2g_{t\varphi,r} \dot{t} \dot{\varphi} - 2g_{rr,\theta} \dot{r} \dot{\theta} + 2\alpha \frac{\partial {}^*RR}{\partial r} \right), \quad (12)$$

$$\ddot{\theta} = \frac{1}{2} g^{\theta\theta} \left(g_{tt,\theta} \dot{t}^2 + g_{rr,\theta} \dot{r}^2 - g_{\theta\theta,\theta} \dot{\theta}^2 + g_{\varphi\varphi,\theta} \dot{\varphi}^2 + 2g_{t\varphi,\theta} \dot{t} \dot{\varphi} - 2g_{\theta\theta,r} \dot{r} \dot{\theta} + 2\alpha \frac{\partial {}^*RR}{\partial \theta} \right), \quad (13)$$

where

$$E = -(g_{tt} \dot{t} + g_{t\varphi} \dot{\varphi}), \quad L_z = g_{\varphi\varphi} \dot{\varphi} + g_{t\varphi} \dot{t}. \quad (14)$$

In addition, the motion of the coupled scalar particle also satisfies the constrain condition

$$h = g_{tt} \dot{t}^2 + g_{rr} \dot{r}^2 + g_{\theta\theta} \dot{\theta}^2 + g_{\varphi\varphi} \dot{\varphi}^2 + 2g_{t\varphi} \dot{t} \dot{\varphi} + 1 - 2\alpha {}^*RR = 0. \quad (15)$$

As in the Kerr case [26], the CS invariant (10) results in the differential equation (15) not being variable-separable. Therefore, the motion of the scalar particle may exhibit the chaotic behavior due to its interaction with the CS invariant. In the next section, we explore the effects of the dilaton parameter D together with the coupling parameter α and the spin parameter a on the motion of the coupled scalar particles in the EMDA black hole spacetime (8).

III. CHAOTIC MOTION OF SCALAR PARTICLES COUPLING TO CHERN-SIMONS INVARIANT IN THE STATIONARY AXISYMMETRIC EMDA BLACK HOLE

We are now to probe the chaotic motion of scalar particles coupling to the CS invariant in the stationary axisymmetric EMDA black hole spacetime. Chaos is highly sensitive to initial values, so the tiny error can yield enormous deviations as the dynamical system is in a chaotic state. To avoid the pseudo-chaos arising from errors in numerical calculations, we here adopt the corrected fifth-order Runge-Kutta method [31, 32] to solve differential equations (11)-(13), which effectively ensures the high precision because at every integration step the numerical deviation is pulled back in a least-squares shortest path by correcting the velocities $(\dot{r}, \dot{\theta})$.

It is well known that the motion of the particle is entirely determined by its initial conditions and the parameters of the system. Generally, the choice for the parameters and initial conditions of the particle should be arbitrary in the allowed range in physics. For a convenience, we here set a regular orbit in the noncoupling case as the initial motion orbit of the particle and then probe the change of the disorder degree of the particle orbit with the coupling, the spin and the dilaton parameters. Here, the selected regular orbit can be obtained by setting the parameters $\{ E = 0.95, M_{ADM} = 1, L = 3.05M, a = 0.31, D = -0.23 \}$ and the initial conditions $\{ r(0) = 11.5, \dot{r}(0) = 0, \theta(0) = \frac{\pi}{2} \}$.

Poincaré section is an effective method to discern the chaos because strange patterns of dispersed points with complex boundaries appear for the chaotic motion in the section. Fig. 1 presents the changes of the Poincaré section ($\theta = \frac{\pi}{2}$) in the $r - \dot{r}$ plane with different CS coupling parameters α . As $\alpha < 61$, we find that the phase path of the coupled scalar particle in the Poincaré section is a quasi-periodic Kolmogorov-Arnold-Moser (KAM) tori, which means that the motion of the particle is regular since its orbit moves on a torus in the phase space. Moreover, with the increase of α , the KAM tori becomes progressively distorted. Especially, as $\alpha = 40$, there is an island chain consisting of three secondary KAM toris, which belong to the same trajectory. When the CS coupling parameter is further increased to $\alpha = 61$, one can find that the KAM tori is destroyed and many discrete points are randomly distributed in the section, which means that the motion of the particle

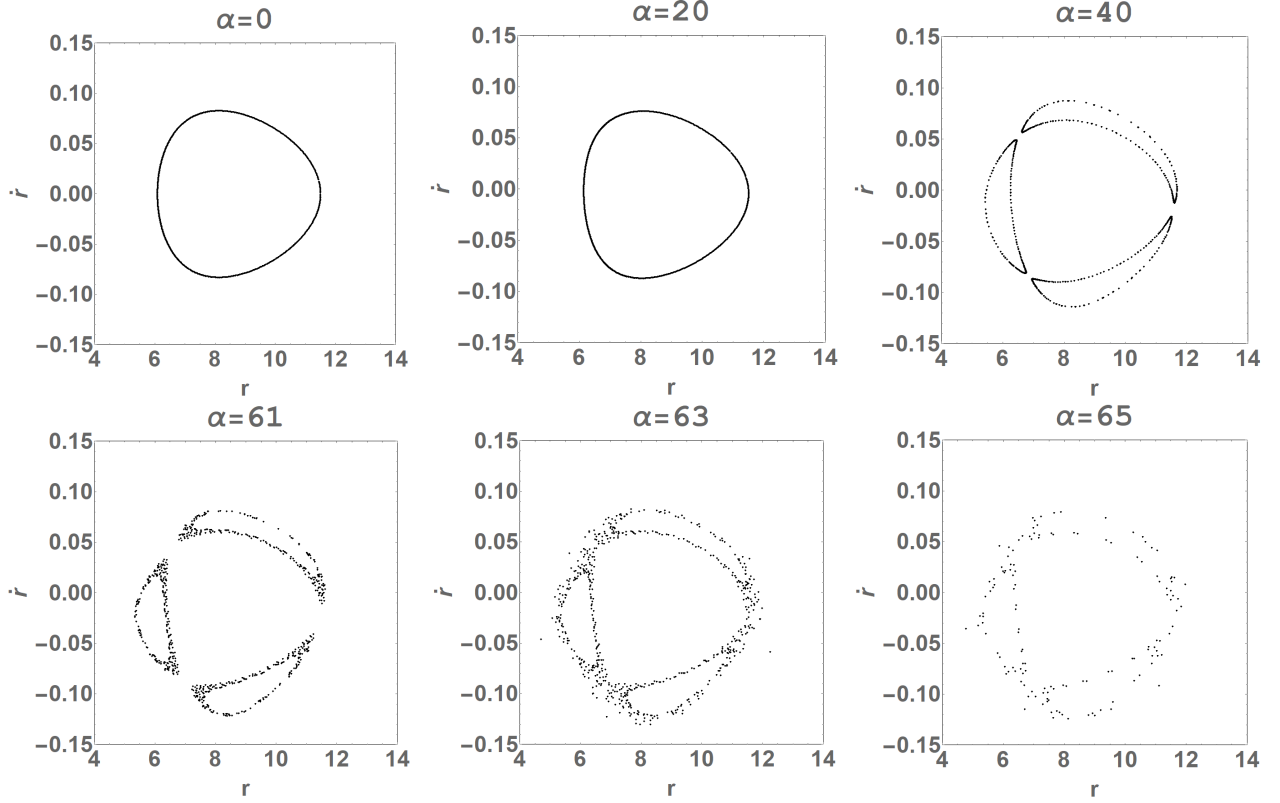


FIG. 1: The Poincaré section ($\theta = \frac{\pi}{2}$) with the coupling parameter α for the motion of a scalar particle coupling to the CS invariant in the stationary axisymmetric EMDA black hole for the fixed values of $r = 11.5$, $a = 0.31$, $D = -0.23$, $M_{ADM} = 1$, $E = 0.95$ and $L = 3.05M$.

is chaotic because its orbit is not limited to the original KAM torus as in regular motions. As $\alpha = 65$, we find that the number of discrete points in the Poincaré section decreases, which is caused by that the particles undergoing chaotic oscillations eventually fall into the black hole's event horizon or escapes to the spatial infinity. Therefore, the coupling of the CS invariant makes the motion of scalar particles more complex.

In Figs. 2-4, we present the Poincaré section ($\theta = \frac{\pi}{2}$) containing nine motion orbits of the coupled particles in the background of a stationary axisymmetric EMDA black hole. We find that the changes of the regular orbit number and chaotic orbit number depend on the black hole parameters a , D and the coupling parameter α . For the fixed spin parameter $a = 0.31$ and dilaton parameter $D = -0.23$, we find that all of nine orbits are regular as $\alpha = 0$ because in this case the motion equations of scalar test particles reduce to the usual variable-separable geodesic equations. With the increase of α , the number of regular motion orbits shrinks and the number of chaotic orbits increases, which is similar to that in the Kerr black hole case [26]. Moreover, we also find that the chaotic orbits are farther from the central fixed point than the regular orbits. For the fixed $\alpha = 55$ and $D = -0.23$, when $a = 0$, one can find that there exist only the regular orbits and the chaos does not occur as in the case $\alpha = 0$, which is because that the CS invariant $*RR$ contains a factor of a and it

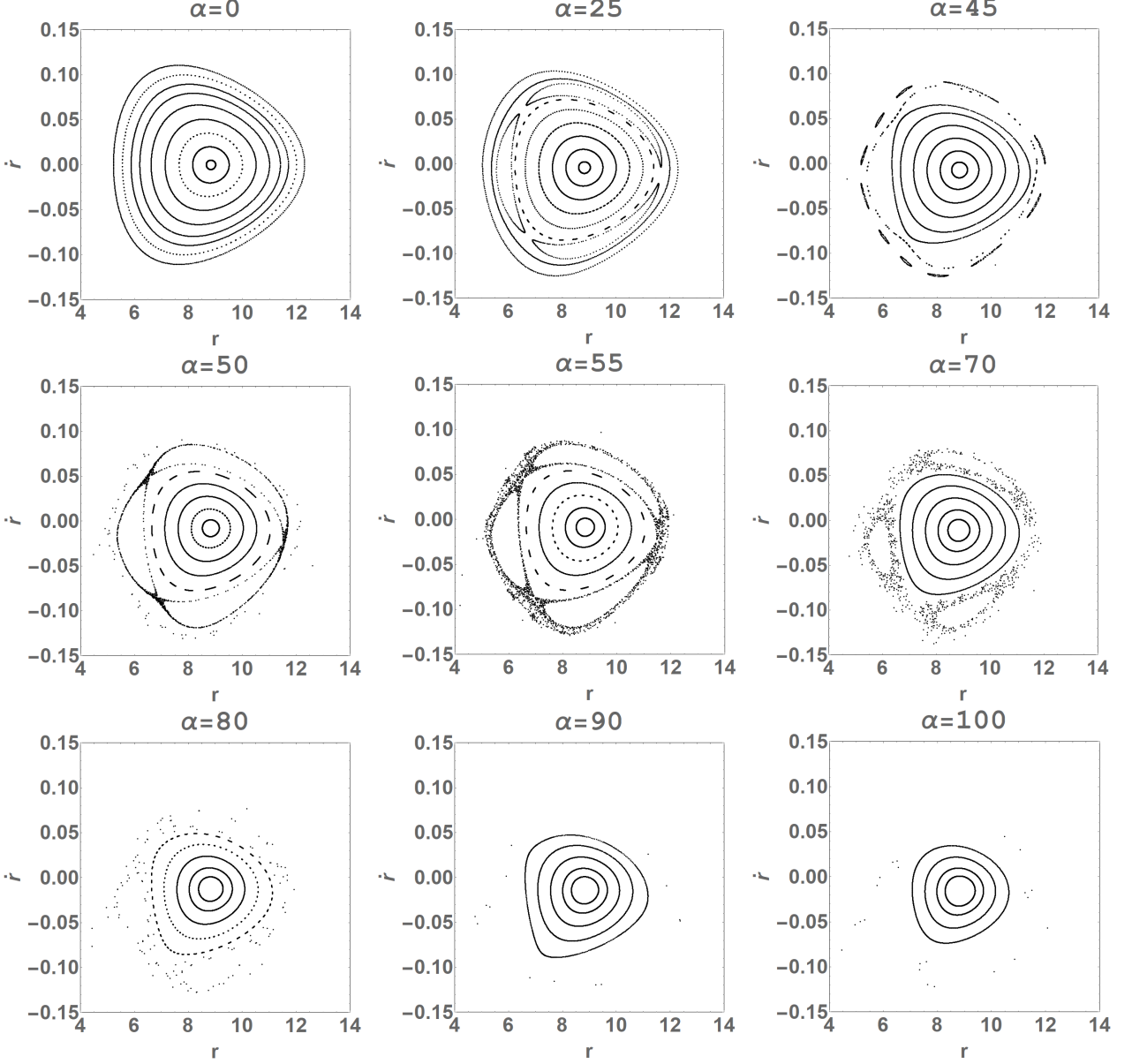


FIG. 2: The Poincaré section ($\theta = \frac{\pi}{2}$) with the coupling parameter α for the motion of the scalar particle coupling to the CS invariant in the stationary axisymmetric EMDA black hole for the fixed parameters $a = 0.31$, $D = -0.23$, $M_{ADM} = 1$, $E = 0.95$ and $L = 3.05M$.

disappears for the static black hole. With the increase of the spin parameter a of the black hole, we find that the number of regular orbits first decreases and then increases. For the fixed $\alpha = 55$ and $a = 0.31$, increasing the absolute value of dilaton parameter D , we observe that the number of regular orbits first increases and then decreases, and finally increases again. Meanwhile, the number of chaotic orbits first increases and then decreases. Moreover, with the increasing α , a and $|D|$, we also find the chaotic strength for the chaotic orbits first increases and then decreases. Thus, the coupling together with the spin and dilaton parameters yields the richer dynamical behavior of the scalar particle in the stationary axisymmetric EMDA black hole spacetime.

As in the Kerr case [26], we also note from Figs. 1-4 that the patterns in the Poincaré section lose the reflection symmetry along the axial line $\dot{r} = 0$ due to the interaction with the CS invariant, which could be a common feature for the particle motions under such a coupling. This can be attributed to that the CS invariant *RR (10) is not symmetric with respect to the equatorial plane.

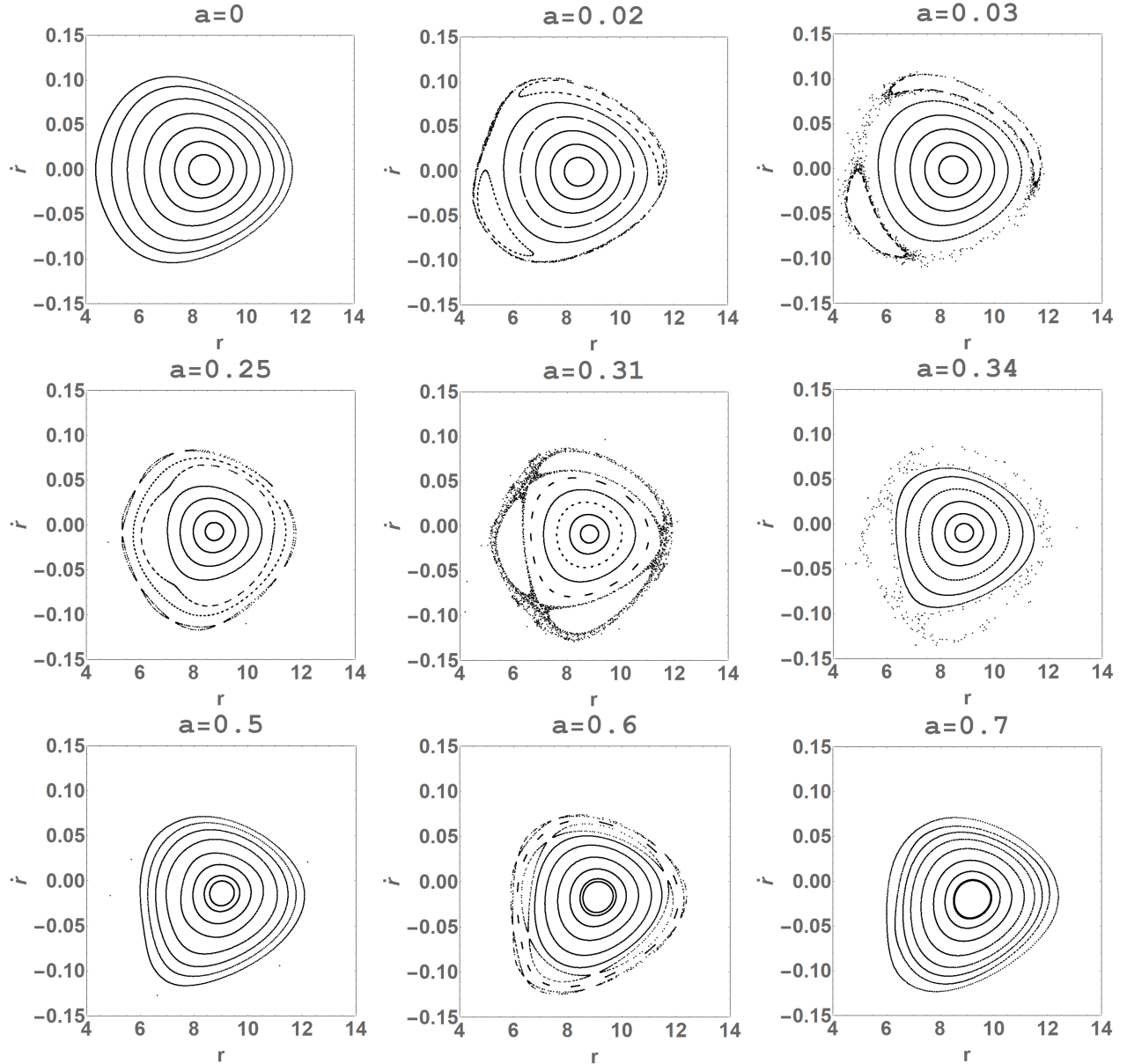


FIG. 3: The Poincaré section ($\theta = \frac{\pi}{2}$) with the spin parameter a for the motion of the scalar particle coupling to the CS invariant in the stationary axisymmetric EMDA black hole for the fixed parameters $\alpha = 55$, $D = -0.23$, $M_{ADM} = 1$, $E = 0.95$ and $L = 3.05M$.

FLI is a fast and efficient tool to identify the chaotic behavior of the particle. In a curved spacetime, the FLI with the two-particle method can be expressed by [33–36]

$$FLI(\tau) = -(k + 1) * \log_{10} d(0) + \log_{10} d(\tau), \quad (16)$$

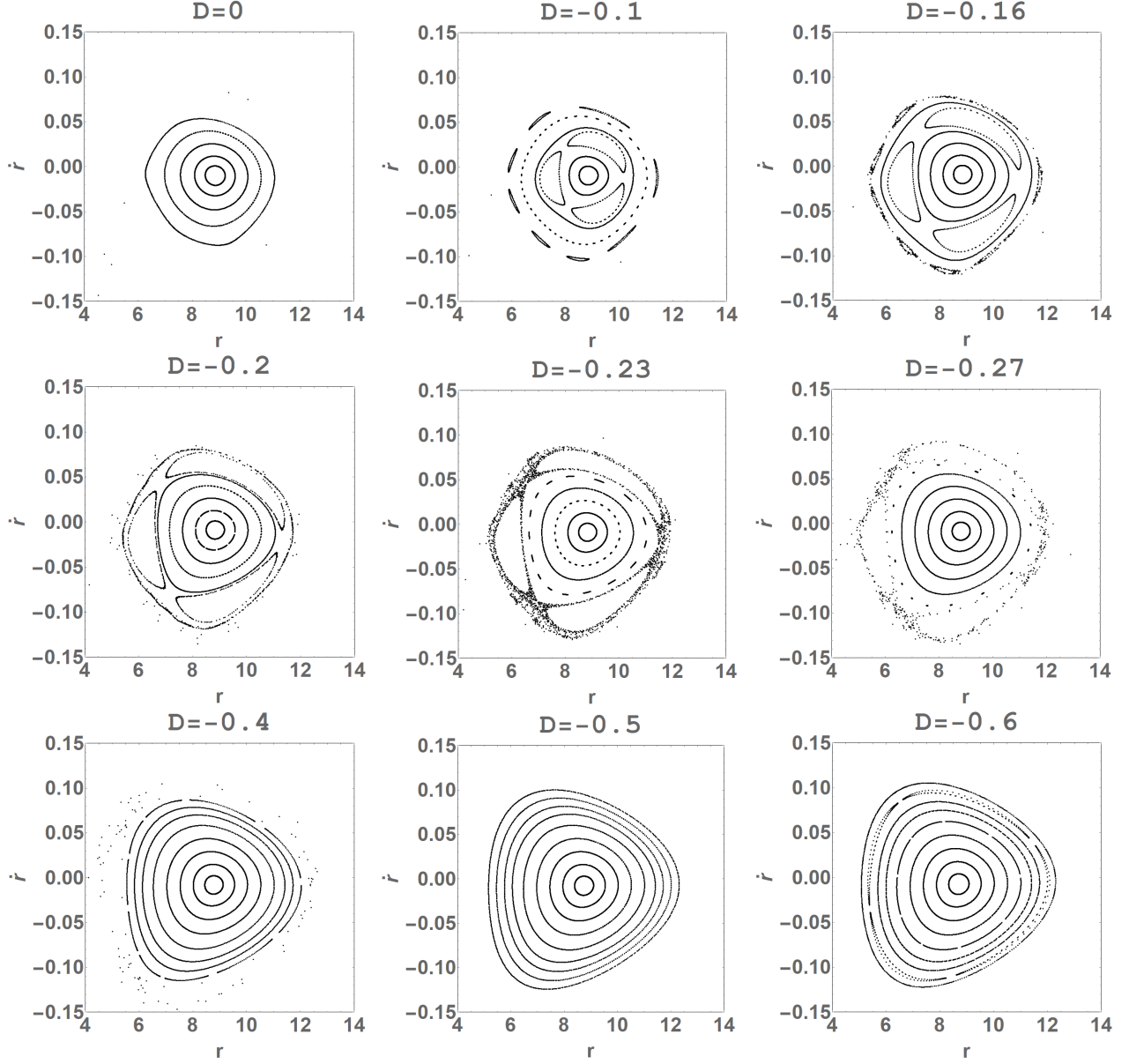


FIG. 4: The Poincaré section ($\theta = \frac{\pi}{2}$) with the dilaton parameter D for the motion of the scalar particle coupling to the CS invariant in the stationary axisymmetric EMDA black hole for the fixed parameters $\alpha = 55$, $a = 0.31$, $M_{ADM} = 1$, $E = 0.95$ and $L = 3.05M$.

where $d(\tau) = \sqrt{|g_{\mu\nu}\Delta x^\mu\Delta x^\nu|}$, Δx^μ is the deviation vector between two adjacent trajectories. To avoid numerical saturation caused by the rapid separation of two adjacent trajectories, the sequential number of renormalization k is introduced. Whenever $d(\tau) = 1$, the value of k is increased by one and then $d(\tau)$ is pulled back to a distance of $d(0)$. The $FLI(\tau)$ grows exponentially for chaotic orbits, but it grows algebraically with time for the regular orbits. In Fig. 5, we present the variation of $FLI(\tau)$ with the coupling parameter α for the initial orbit selected in Fig. 1. It shows that the $FLI(\tau)$ increases linearly with τ as $\alpha < 61$, which means that the motion of the scalar particle is regular in this case. However, in the case of $\alpha \geq 61$, the $FLI(\tau)$ grows

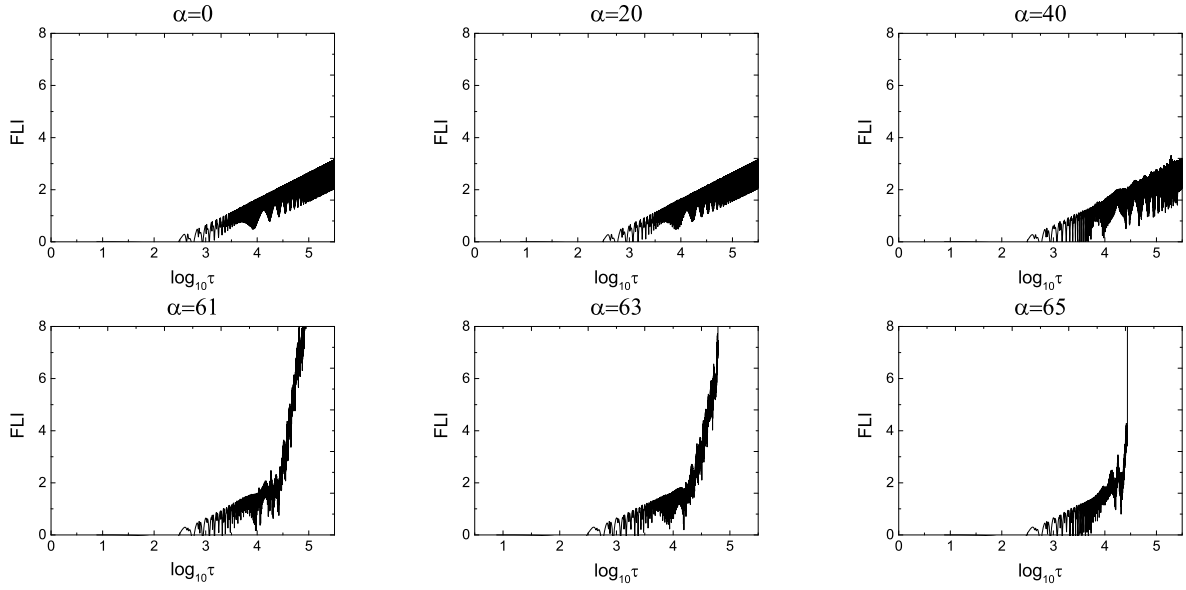


FIG. 5: The fast Lyapunov Indicator (FLI) with the coupling parameter α for the signals shown in Fig. 1.

exponentially with τ , and the corresponding motion is chaotic. These results agree with those obtained from the Poincaré section shown in Fig. 1.

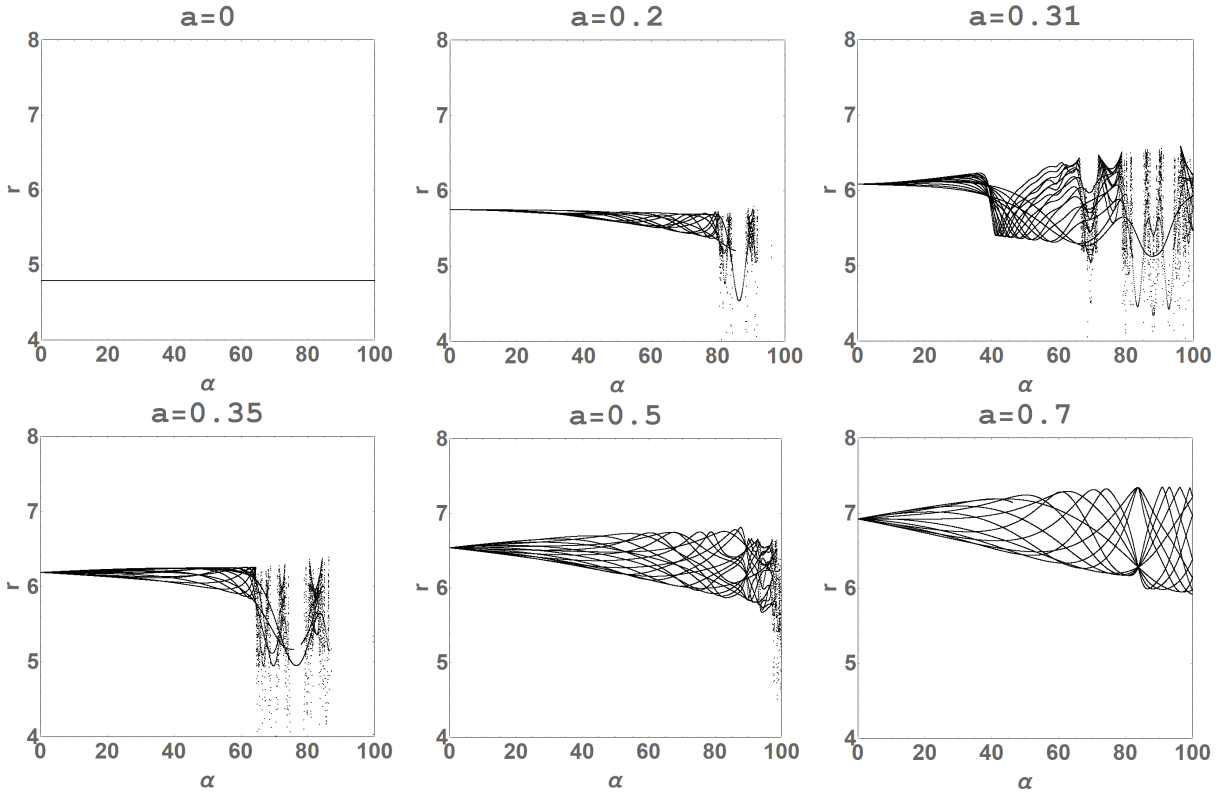


FIG. 6: The bifurcation changes with the CS coupling parameter α for the fixed dilaton parameter $D = -0.23$ and different spin parameters a .

The bifurcation diagram can illustrate the dependence of dynamical behaviors of the particle motion on

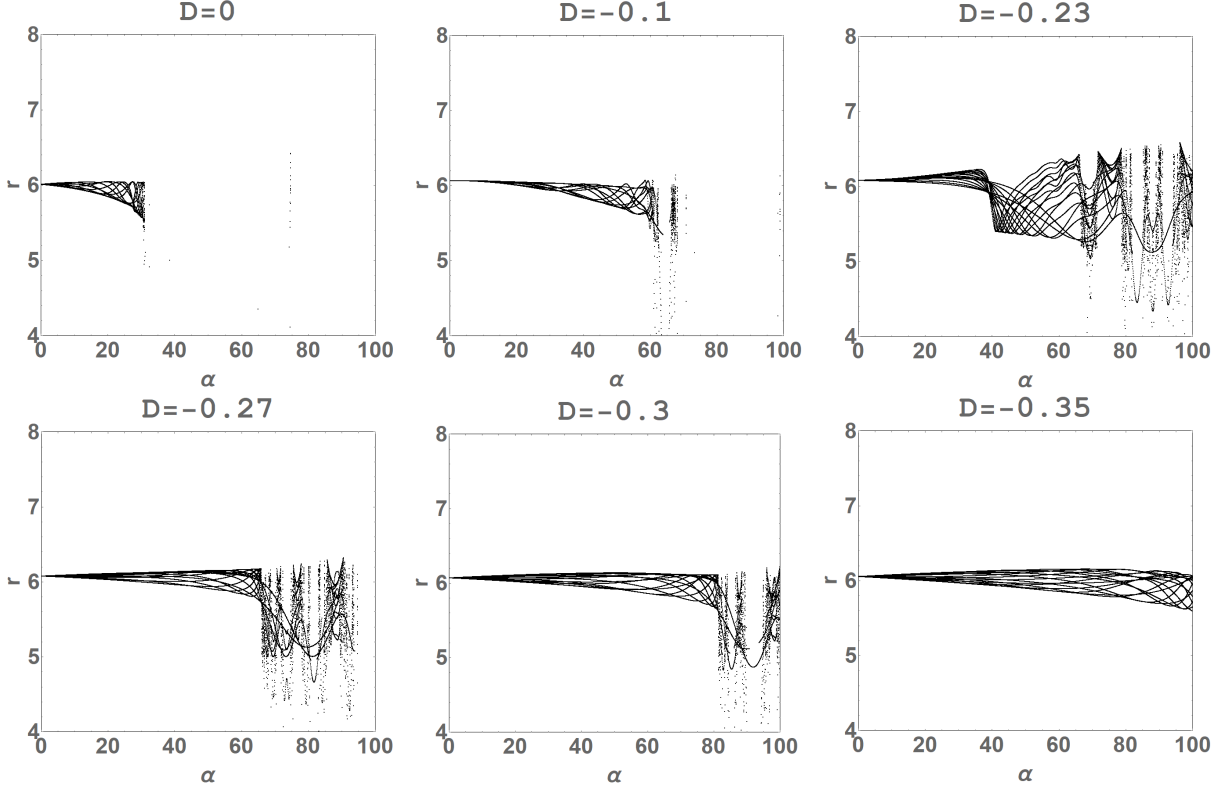


FIG. 7: The bifurcation changes with the CS coupling parameter α for the fixed spin parameter $a = 0.31$ and different dilaton parameters D .

system parameters. In Figs. 6-9, we plot the bifurcation diagram of the radial coordinate of the particle in the EMDA black hole spacetime, and probe effects of the CS coupling parameter α , the spin parameter a , and the dilaton parameter D on the motion of particles. When $\alpha = 0$ or $a = 0$, one can find that there is no bifurcation for dynamical systems and the motion of the scalar particle is regular in both cases. For the fixed dilaton parameter $D = -0.23$, with the increase of the spin parameter a of the black hole, Fig. 6 shows that the range of α where the chaos occurs first increases and then decreases, and the corresponding lower limit of α first decreases and then increases. For the fixed spin parameter $a = 0.31$, with the increasing $|D|$, Fig. 7 shows that the range of α where the chaos appears decreases and the lower limit of α increases. With the increase of α , Fig. 8 illustrates that the range of D where the chaos occurs increases and the corresponding lower limit of D decreases. For the fixed $\alpha = 55$, with the increase of $|D|$, Fig. 9 shows that the range of a in which the chaos appears decreases and the corresponding upper limit of a decreases. These indicate that the motions of the coupled scalar particles heavily depend on the coupling parameter α , the black hole parameters a and D . Therefore, under the interaction with the CS invariant, the dynamical behavior becomes much richer in a usual rotating EMDA black hole spacetime.

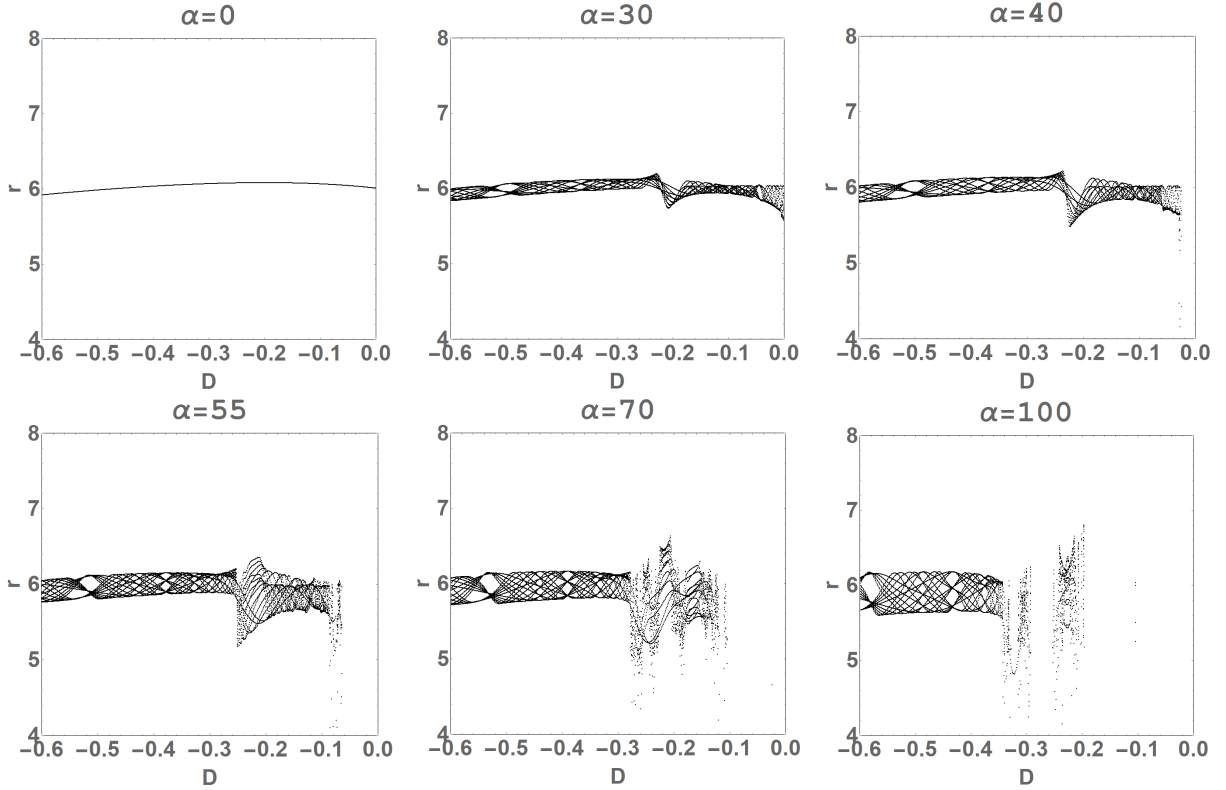


FIG. 8: The bifurcation changes with the dilaton parameter D for the fixed spin parameter $a = 0.31$ and different values of the CS coupling parameter α .

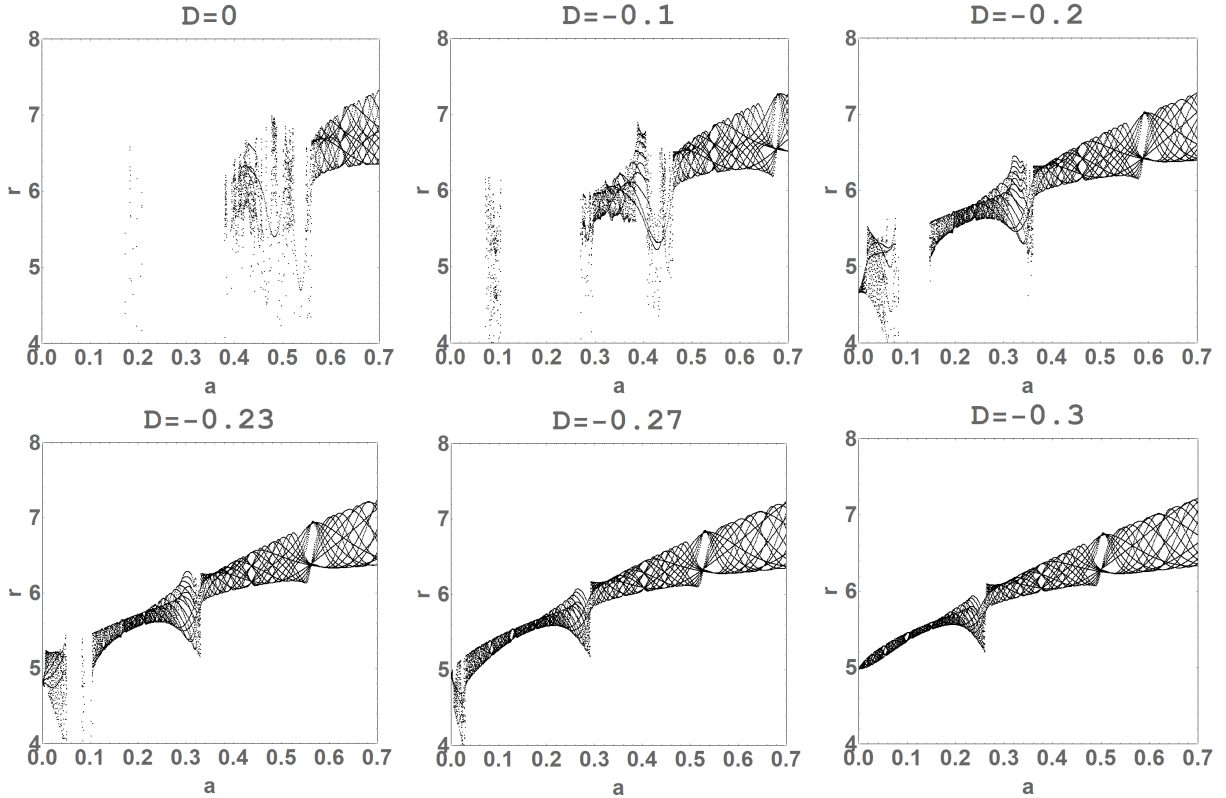


FIG. 9: The bifurcation changes with the spin parameter a for the fixed CS coupling parameter $\alpha = 55$ and different values of the dilaton parameter D .

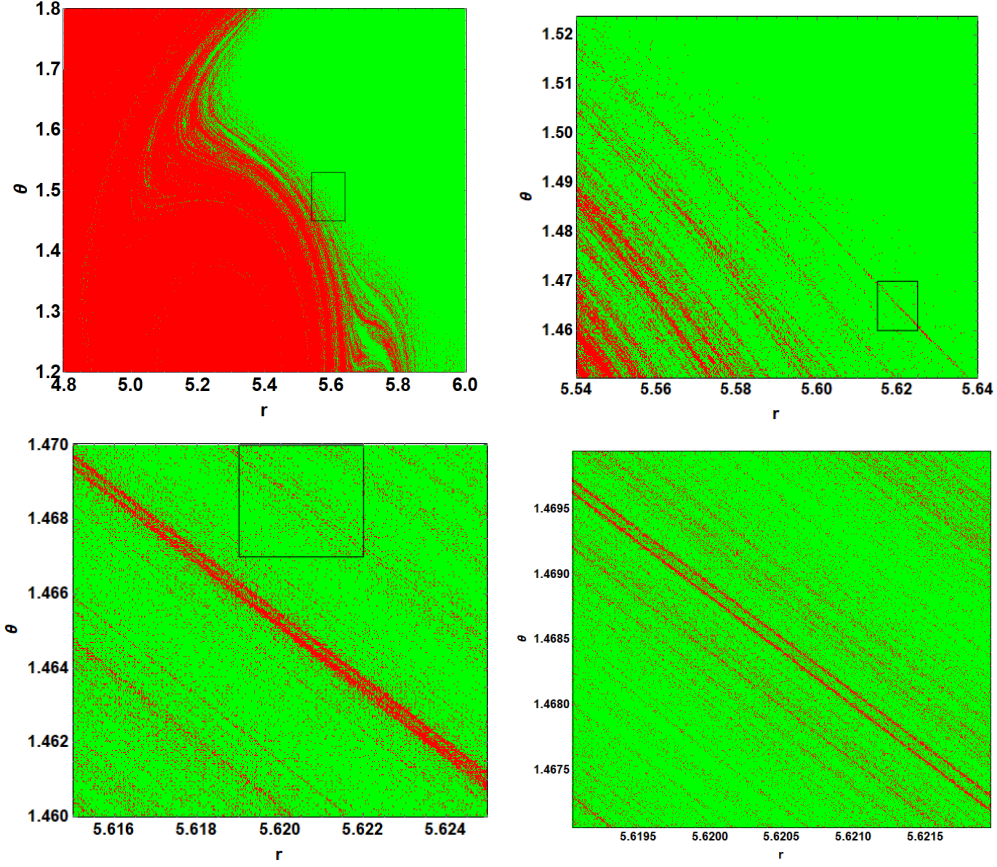


FIG. 10: The fractal basins of attraction for the coupled scalar particle in a stationary axisymmetric EMDA black hole spacetime with the fixed parameters $D = -0.23$, $a = 0.31$, $\alpha = 55$, $M_{ADM} = 1$, $M = M_{ADM} + D$, $E = 0.95$ and $L = 3.05M$.

Analysing the basin boundaries of attractors [37–39] can help to identify the signatures of chaos because the boundary between basins can be fractal as the chaos is present. In Fig. 10, we plot the basins of attraction in a large subset of phase space for a coupled scalar particle in a stationary axisymmetric EMDA black hole spacetime with the fixed parameters $\alpha = 55$, $a = 0.31$, $D = -0.23$, $M_{ADM} = 1$, $E = 0.95$ and $L = 3.05M$. The initial conditions corresponding to the points shown in the figure, are set to $\dot{r} = 0$, and then $\dot{\theta}$ is given by the constraint (15), i.e., $h = 0$. The red point corresponds to the particle falling into the black hole along geodesics. The blue point represents the particle escaping into infinity, and the green point denotes the particle oscillating around the black hole. Here, the condition for the captured particle is set to be $r \leq r_+$ and the condition for the escape is to be $r \geq 100r_+$. For the green dots, we consider trajectories that neither get captured nor escaped to infinity within 100,000 iterations. In Fig. 10, it is easy to find that there exist some self-similar fractal fine structures in the basins boundaries attractors, which also means that there exists the chaotic motion for a coupled scalar particle in the stationary axisymmetric EMDA black hole spacetime.

IV. SUMMARY

We have studied the motion of test scalar particles coupling to the CS invariant in the stationary axisymmetric EMDA black hole spacetime. The presence of the dilation parameter makes the CS invariant more complex, which yields richer dynamical behaviors of the particles. Applying techniques including the Poincaré section, fast Lyapunov exponent indicator, bifurcation diagram and basins of attraction, we confirmed the presence of chaos in the motion of scalar particles interacting with the CS invariants in the rotating EMDA black hole spacetime. The effects of the coupling parameter α and the spin parameter a on the test scalar particle are similar to those in the Kerr black hole case. With the increasing the absolute value of the dilaton parameter D , the number of regular orbits in the Poincaré section first increases and then decreases, and finally increases again. Meanwhile, the number of chaotic orbits first increases and then decreases. Moreover, with the increasing $|D|$, the chaotic strength for the chaotic orbits first increases and then decreases. For the fixed spin parameter ($a = 0.31$), with the increase of α , we found that the range of D where the chaos occurs increases and the corresponding lower limit of D decreases. With the increasing $|D|$, the range of α for the appearance of the chaos decreases and the lower limit of α increases. For the fixed coupling parameter ($\alpha = 55$), with the increase of $|D|$, we observed that the range of a in which the chaos appears decreases and the corresponding upper limit of a decreases. These indicate that the motions of the coupled scalar particles heavily depend on the coupling parameter α , the black hole parameters a and D . Therefore, the CS invariant coupling together with the spin and dilaton parameters yields the richer dynamical behavior of the scalar particle in the stationary axisymmetric EMDA black hole spacetime.

Acknowledgments

This work was supported by the National Key Research and Development Program of China (Grant No. 2020YFC2201400) and National Natural Science Foundation of China (Grant Nos. 12275078, 12275079 and 12035005).

-
- [1] E. Ott, *Chaos in Dynamical Systems*, Cambridge University Press, Second Edition 2002.
 - [2] R. Brown and L. Chua, Clarifying chaos: examples and counterexamples, *Int. J. Bifurcation and Chaos* **6**, 219 (1996).
 - [3] R. Brown and L. Chua, Clarifying chaos II: Bernoulli chaos, zero Lyapunov exponents and strange attractors, *Int. J. Bifurcation and Chaos* **8**, 1 (1998).

- [4] C. Dettmann, N. Frankel, and N. Cornish, Fractal basins and chaotic trajectories in multi-black-hole spacetimes, *Phys. Rev. D* **50**, R618 (1994).
- [5] D. Li and X. Wu, Chaotic motion of neutral and charged particles in a magnetized Ernst-Schwarzschild spacetime, *Eur. Phys. J. Plus* **134**, 96 (2019).
- [6] S. Chen, M. Wang, and J. Jing, Chaotic motion of particles in the accelerating and rotating black holes spacetime, *J. High Energy Phys.* **09**, 082 (2016).
- [7] M. Wang, S. Chen, and J. Jing, Chaos in the motion of a test scalar particle coupling to the Einstein tensor in Schwarzschild-Melvin black hole spacetime, *Eur. Phys. J. C* **77**, 208 (2017).
- [8] M. Chabab, H. Moumni, S. Iraoui, K. Masmar, and S. Zhizeh, Chaos in charged AdS black hole extended phase space, *Phys. Lett. B* **781**, 316 (2018).
- [9] Y. Chen, H. Li, and S. Zhang, Chaos in Born-Infeld-AdS black hole within extended phase space, *Gen. Rel. Grav.* **51**, 134 (2019).
- [10] S. Mahish and B. Chandrasekhar, Chaos in Charged Gauss-Bonnet AdS Black Holes in Extended Phase Space, *Phys. Rev. D* **99**, 106012 (2019).
- [11] C. Dai, S. Chen, and J. Jing, Thermal chaos of a charged dilaton-AdS black hole in the extended phase space, *Eur. Phys. J. C* **80**, 245 (2020).
- [12] C. Will, The confrontation between general relativity and experiment, *Living Rev. Rel.* **17**, 4 (2014).
- [13] E. Berti et al., Testing general relativity with present and future astrophysical observations, *Class. Quant. Grav.* **32**, 243001 (2015).
- [14] S. Alexander and N. Yunes, Chern-Simons Modified General Relativity, *Phys. Rep.* **480**, 1 (2009).
- [15] T. Shiromizu and K. Tanabe, Static spacetimes with/without black holes in dynamical Chern-Simons gravity, *Phys. Rev. D* **87**, 081504 (2013).
- [16] N. Yunes and F. Pretorius, Dynamical Chern-Simons modified gravity: Spinning black holes in the slow-rotation approximation, *Phys. Rev. D* **79**, 084043 (2009).
- [17] K. Konno, T. Matsuyama, and S. Tanda, Rotating Black Hole in Extended Chern-Simons Modified Gravity, *Prog. Theor. Phys.* **122**, 561 (2009).
- [18] K. Yagi, N. Yunes, and T. Tanaka, Slowly rotating black holes in dynamical Chern-Simons gravity: Deformation quadratic in the spin, *Phys. Rev. D* **86**, 044037 (2012).
- [19] G. Nashed and S. Nojiri, Slow-rotating charged black hole solution in dynamical Chern-Simons modified gravity, *Phys. Rev. D* **107**, 064069 (2023).
- [20] G. Nashed and S. Capozziello, Spinning (A)dS black holes with slow-rotation approximation in dynamical Chern-Simons modified gravity, *Phys. Rev. D* **107**, 063008 (2023).
- [21] K. Konno and R. Takahashi, Scalar field excited around a rapidly rotating black hole in Chern-Simons modified gravity, *Phys. Rev. D* **90**, 064011 (2014).
- [22] G. Antoniou, A. Bakopoulos, and P. Kanti, Evasion of No-Hair Theorems and Novel Black-Hole Solutions in Gauss-Bonnet Theories, *Phys. Rev. Lett.* **120**, 131102 (2018).
- [23] D. Doneva and S. Yazadjiev, New Gauss-Bonnet Black Holes with Curvature-Induced Scalarization in Extended Scalar-Tensor Theories, *Phys. Rev. Lett.* **120**, 131103 (2018).
- [24] H. Silva, J. Sakstein, L. Gualtieri, T. Sotiriou, and E. Berti, Spontaneous Scalarization of Black Holes and Compact Stars from a Gauss-Bonnet Coupling, *Phys. Rev. Lett.* **120**, 131104 (2018).

- [25] Y. Gao, Y. Huang, and D. Liu, Scalar perturbations on the background of Kerr black holes in the quadratic dynamical Chern-Simons gravity, *Phys. Rev. D* **99**, 044020 (2019).
- [26] X. Zhou, S. Chen, and J. Jing, Chaotic motion of scalar particle coupling to Chern-Simons invariant in Kerr black hole spacetime, *Eur. Phys. J. C* **81**, 233 (2021).
- [27] A. Sen, Rotating charged black hole solution in heterotic string theory, *Phys. Rev. Lett.* **69**, 1006 (1992).
- [28] A. Garcia, D. Galtsov, and O. Kechkin, Class of stationary axisymmetric solutions of the Einstein-Maxwell dilaton-axion field equations, *Phys. Rev. Lett.* **74**, 1276 (1995).
- [29] Q. Pan and J. Jing, Quasinormal frequencies and thermodynamic instabilities for the stationary axisymmetric Einstein-Maxwell dilaton-axion black hole, *J. High Energy Phys.* **01**, 044 (2007).
- [30] J. Jing and S. Wang, Can Martinezs conjecture be extended to string theory? *Phys. Rev. D* **65**, 064001 (2002).
- [31] D. Ma, X. Wu, and J. Zhu, Velocity scaling method to correct individual Kepler energies, *New Astron.* **13**, 216 (2008).
- [32] D. Ma, X. Wu, and F. Liu, Velocity corrections to Kepler energy and Laplace integral, *Int. J. Mod. Phys. C* **19**, 1411 (2008).
- [33] G. Tancredi, A. Sánchez, and F. Roig, A Comparison Between Methods to Compute Lyapunov Exponents, *Astron. J.* **121**, 1171 (2001).
- [34] C. Froeschlé and E. Lega, On the Structure of Symplectic Mappings. The Fast Lyapunov Indicator: a Very Sensitive Tool, *Celest. Mech. Dyn. Astron.* **78**, 167 (2000).
- [35] X. Wu, T. Huang, and H. Zhang, Lyapunov indices with two nearby trajectories in a curved spacetime, *Phys. Rev. D* **74**, 083001 (2006).
- [36] Y. Chen and X. Wu, Application of force gradient symplectic integrators to the circular restricted three-body problem, *Acta Phys. Sin.* **14**, 140501 (2013).
- [37] C. Dettmann, N. Frankel, and N. Cornish, Fractal basins and chaotic trajectories in multi-black-hole spacetimes, *Phys. Rev. D* **50**, R618 (1994).
- [38] A. Frolov and A. Larsen, Chaotic scattering and capture of strings by black hole, *Class. Quant. Grav.* **16**, 3717 (1999).
- [39] S. McDonald, C. Grebogi, E. Ott, and J. Yorke, Fractal Basin Boundaries, *Physica D* **7**, 125 (1985).